# The Effect of Adsorption on Mass Transfer in Fluidized Bed Catalytic Reactors

**İnci Akşahin, İnci Eroğlu* and Hayrettin Yücel**

*Department of Chemical Engineering, Middle East Technical University, Ankara 06531, Turkey*

Tracer gas residence time distributions (RTD) in a laboratory scale fluidized bed system have been measured for pulses of three different tracer gases (methane, ethane and propane) at different temperatures in the range 323 to 435 K. The fluidized solid was a commercial zeolite based FCC catalyst (CBZ-2), and measurements were carried out in a superficial air velocity range of 0.01 to 0.04 m/s. The data were interpreted with two-phase dense phase dispersion models for adsorptive tracers, available in the literature. In addition, modified models were considered by assuming a stationary dense phase and neglecting axial dispersion in this phase. Mean residence time, $\mu_1$, and the variance of the residence time, $\sigma^2$, of RTD data were calculated for each experimental run. Applying the moment technique in the Laplace domain, the differential equations for all models considered were analytically solved.

Mass transfer coefficients obtained from dynamic experiments were compared with the values estimated from the relations available in the literature. It was found that methods considering convective flux alone between the bubble and emulsion phases give closer values to the experimental ones than the methods also including the diffusive flux.

Les distributions de temps de séjour d'un traceur gazeux dans un système à lit fluidisé à l'échelle de laboratoire ont été mesurées pour des pulsations de trois traceurs (méthane, éthane et propane) à des températures comprises entre 323 et 435 K. Le solide fluidisé est un catalyseur FCC commercial basé sur une zéolite (CBZ-2), et des mesures ont été prises dans une gamme de vitesses d'air superficielles de 0,01 à 0,04 m/s. Les données ont été interprétées à l'aide de modèles de dispersion de phase dense biphasiques publiés pour les traceurs adsorbants. En outre, des modèles modifiés ont été pris en compte en supposant une phase dense stationnaire et en négligeant la dispersion axiale dans cette phase. Le temps de séjour moyen $\mu_1$ et la variance du temps de séjour $\sigma^2$ des données de DTS ont été calculés pour chaque essai expérimental. Les équations différentielles de tous les modèles considérés ont été résolues analytiquement en appliquant la méthode du moment dans le domaine de Laplace.

Des coefficients de transfert de matière provenant d'expériences dynamiques ont été comparés aux valeurs estimées à partir de relations disponibles dans la littérature scientifiques. On a trouvé que les méthodes ne retenant que le flux de convection entre la phase des bulles et la phase d'émulsion donnent des valeurs plus proches des valeurs expérimentales que les méthodes qui tiennent également compte du flux de diffusion.

**Keywords:** fluidized bed, adsorption, mass transfer, residence time distribution, FCC catalyst.

Because of their commercial importance, fluidized bed reactors have received considerable attention in the literature and numerous mathematical models have been proposed to account for and predict their performance (for example, see reviews of Fane and Wen, 1982; Grace, 1985, 1986; van Swaaij, 1985). Many of these models are based on the two-phase concept of fluidization, which assumes that all gas in excess of that required to just fluidize the bed passes through the bed in the form of bubbles. These models, which have been developed by setting up conservation of mass equations at the scale of the reactor, represent the fludized bed system in terms of the hydrodynamic system parameters, mass transfer coefficient between phases, and macromixing behaviour of solid and gas in the system. In the case of heterogeneous fluid bed reactors, one must also consider information about the apparent reaction rate and adsorption equilibrium that are related to the microkinetics of the fluidized bed system at the scale of particles. Tracer gas experiments have long been used to characterize homogeneous and heterogeneous fluid bed reactors. However in the case of heterogeneous fluid bed reactors, it is much more difficult to interpret the results because of their sensitivity to the extent of tracer partition between the phases, which is generally termed as the adsorption coefficient. Several investigators used residence time distribution measurements to analyze both solids and gas dynamics in fluidized beds and to elucidate the influence of adsorption on mass transfer between phases and reactor performance (Yoshida and Kunii, 1968; Zalewski and Hanesian, 1973; Drinkenburg and Rietema, 1973; Morooka et al., 1977; Bohle and van Swaaij, 1978; Kühne and Wippern, 1980; Schlingman et al., 1982; Krambeck et al., 1987; Hatano and Ishida 1990). However, relatively few studies attempted to match the tracer results and mathematical models to predict the reactor performance in freely bubbling conditions (Mooroka et al., 1977; Bohle and van Swaaij, 1978).

It is obvious that more information about the mixing behaviour of the system and the influence of adsorption on mass transfer between phases can be obtained by using several tracers of different adsorption coefficients. Furthermore, the adsorption coefficient of the given gas can be changed by varying the temperature. The present study investigates the effect of adsorption on mass transfer in a laboratory scaled fluidized bed reactor by employing different tracer gases that have different adsorptivities on a commercial cracking catalyst. Furthermore, the temperature was varied to observe the effect of temperature on mass transfer for systems involving adsorptive tracers in an attempt to shed more light on the mechanism for mass transfer in these systems.

## Fluidized Bed Models

In the present study, two dynamic flow models for adsorbing tracers proposed by Bohle and van Swaaij (1978) and Morooka et al. (1977) were considered. These models were the extensions of two-phase

*Author to whom correspondence may be addressed. E-mail address: ieroglu@metu.edu.tr

models presented by May (1959) and van Deemter (1961) for nonadsorbing tracers. The basic differences between the models of Bohle and van Swaaij and Morooko et al. arise from the interpretation of the mixing behaviour of gas and solids in the dense phase and the definition of the adsorption equilibrium constant.

In the study of Bohle and van Swaaij (1978), the gas mixing in the emulsion phase was described by an axially dispersed plug flow model. It was assumed that the axial dispersion coefficient of gas in the emulsion phase, *Eg*, is equal to the axial dispersion coefficient of particles in the emulsion phase, $E_s$. In their work, the adsorption equilibrium constant was defined as:

$$m_B = \frac{m}{\varepsilon_b(1-\phi)} \tag{1}$$

where $m$ is the adsorption equilibrium constant, which is equivalent to the adsorption equilibrium constant obtained from gas chromatography experiments, and $\varepsilon_b(1-\phi)$ is the fraction of fluidized bed occupied by voidages other than the bubbles.

In the study of Morooka et al. (1977), the mixing behaviour of adsorptive gas in the emulsion phase involves the adsorptive capacitance effect proposed by Miyauchi (1968). The diffusional flux of gas is combined with the diffusional flux of particles to give the overall axial dispersion coefficient for the gaseous component in the emulsion phase, $E_e$, as follows:

$$E_e = E_s\,(\varepsilon_{fe}/\varepsilon_{se} + m_m) \tag{2}$$

where $\varepsilon_{fe}$ and $\varepsilon_{se}$ are the void and solid fractions in dense phase, respectively. Adsorption equilibrium constant, $m_m$, is defined as:

$$m_m = \varepsilon_p + \frac{m}{(1-\delta)(1-\varepsilon_{mf})} \tag{3}$$

where $\varepsilon_{mf}$ and $\varepsilon_p$ are the minimum fluidization and particle porosities, respectively, and $\delta$ is the volume fraction of fluidized bed occupied by bubbles.

In the present study two modified models were also considered. These models were obtained from models of Bohle and van Swaaij (1978) and Morooka et al. (1977) by making two assumptions: (1) axial dispersion in the emulsion phase is neglected; and (2) no net vertical gas flow in the emulsion phase (stagnant emulsion phase) is assumed. These models are abbreviated in the rest of the paper as follows: Bohle and van Swaaij (BVS), Morooka et al. (M), modified Bohle and van Swaaij (M-BVS) and modified Morooka et al. (M-M).

The basic assumption of these two-phase models is that all gas in excess of that required to just fluidize the bed passes through the bed in the form of bubbles. This assumption does not completely hold, and reported values for visible bubble flow rate are typically 10% lower for A-type particles, which include FCC catalysts (Clift, 1986). Furthermore, dense phase velocity is independent of minumum fluidization velocity for this kind of particle (Morooka, 1972). These limitations might be considered in the interpretation of experimental data.

For each of the four models considered, the transient conservation of mass equations for the tracer gas, along with the initial and boundary conditions, are given in Table 1. The model parameters are also included in this table.

The solution of these equations in the Laplace domain by the moment technique with the method of van der Laan (1958) gives the expressions for the first absolute moment and the second central moment. These are the mean residence time, $\mu_1$, and the variance of residence time, $\sigma^2$, of the adsorptive tracer gases in the fluidized bed reactor. The details of the solution are given in Akşahin (1993), and a shorter description of the mathematics for BVS model is presented in the Appendix. The expressions for $\mu_1$ and $\sigma^2$ are given in Table 2.

## Gas Interchange Coefficients

The gas interchange coefficient is an important model parameter evaluated in the present work. For comparison, this parameter can also be estimated from the relations available in the literature. Hence a short review of these relations is given below.

According to the bubbling bed model proposed by Kunii and Levenspiel (1969), the rates of interchange of the gaseous component between bubble and emulsion phases based on unit volume of bubble are given as:

$$-\frac{1}{V_b}\frac{dN_B}{dt} = (K_{be})_b(C_b - C_e) \tag{4}$$

$$-\frac{1}{V_b}\frac{dN_B}{dt} = (K_{bc})_b(C_b - C_c) \tag{5}$$

$$-\frac{1}{V_b}\frac{dN_B}{dt} = (K_{ce})_b(C_c - C_e) \tag{6}$$

The interchange coefficient between bubble and cloud $(K_{bc})_b$, cloud and emulsion $(K_{ce})_b$, and the overall coefficient between bubble and emulsion $(K_{be})_b$ are related as follows:

$$\frac{1}{(K_{be})_b} = \frac{1}{(K_{bc})_b} + \frac{1}{(K_{ce})_b} \tag{7}$$

The mass transfer between bubble and emulsion phases can also be defined in terms of the mass transfer coefficient $(k_{be})$ based on the interphase area $(S_{be})$ as:

$$-\frac{1}{S_{be}}\frac{dN_B}{dt} = k_{be}(C_b - C_e) \tag{8}$$

Interfacial area per unit volume of bubble ($a$) and per unit volume of bed ($a_b$), and volume fraction of bubble phase ($\delta$) for a spherical bubble are related as follows:

$$a_b = \frac{6}{d_b}\delta \tag{9}$$

$$a = \frac{S_{be}}{V_b} = \frac{6}{d_b} \tag{10}$$

Consequently, the overall gas interchange coefficient between bubble and emulsion phases, $(K_{be})_b$ and the overall

**Table 1.** Two-phase models used in the present study.

| Models | (BVS) | (M-BVS) |
|---|---|---|
| **Model Equations** | | |
| Bubble Phase | $\phi\frac{\partial C_b}{\partial\theta}+\frac{\partial C_b}{\partial\zeta}+N_k(C_b-C_e)=0$ | $\phi\frac{\partial C_b}{\partial\theta}+\frac{\partial C_b}{\partial\zeta}+N_k(C_b-C_e)=0$ |
| Emulsion Phase | $(m_B+1)(1-\phi)\frac{\partial C_e}{\partial\theta}+\frac{\partial C_e}{\partial\zeta}+\frac{1}{N_E}\frac{\partial^2 C_e}{\partial\zeta^2}-N_k(C_b-C_e)=0$ | $(m_B+1)(1-\phi)\frac{\partial C_e}{\partial\theta}-N_k(C_b-C_e)=0$ |
| Initial and Boundary Conditions | $\theta=0 \quad C_b=C_e=0$<br>$\theta\geq 0 \quad \zeta=0 \quad \frac{\partial C_e}{\partial\zeta}=0 \quad C_b=\delta(t)$<br>$\zeta=1 \quad \frac{\partial C_e}{\partial\zeta}=0$ | $\theta=0 \quad C_b=C_e=0$<br>$\theta\geq 0 \quad \zeta=0 \quad C_b=\delta(t)$ |
| Model Parameters | $m_B=\frac{m}{\varepsilon_b(1-\phi)}$<br>$N_k=\frac{K_t H_f}{U_o}$<br>$N_e=\frac{U_o H_f}{(m_B+1)(1-\delta)E_s}$ | $m_B=\frac{m}{\varepsilon_b(1-\phi)}$<br>$N_k=\frac{K_t H_f}{U_o}$ |

| Models | (M) | (M-M) |
|---|---|---|
| **Model Equations** | | |
| Bubble Phase | $\frac{\varepsilon\delta}{(1-\delta)(\varepsilon_{fe}+m_m\varepsilon_{se})}\frac{\partial C_b}{\partial\theta'}+\frac{\partial C_b}{\partial\zeta}+N_k(C_b-C_e)=0$ | $\delta\frac{\partial C_b}{\partial\theta'}+\frac{\partial C_b}{\partial\zeta}+N_k(C_b-C_e)=0$ |
| Emulsion Phase | $\varepsilon\frac{\partial C_e}{\partial\theta'}-\frac{1}{Pe_B}\frac{\partial^2 C_e}{\partial\zeta^2}-N_k(C_b-C_e)=0$ | $(1-\delta)(\varepsilon_{fe}+m_m\varepsilon_{se})\frac{\partial C_e}{\partial\theta'}-N_k(C_b-C_e)=0$ |
| Initial and Boundary Conditions | $\theta=0 \quad C_b=C_e=0$<br>$\theta\geq 0 \quad \zeta=0 \quad \frac{\partial C_e}{\partial\zeta}=0 \quad C_b=\delta(t)$<br>$\zeta=1 \quad \frac{\partial C_e}{\partial\zeta}=0$ | $\theta=0 \quad C_b=C_e=0$<br>$\theta\geq 0 \quad \zeta=0 \quad C_b=\delta(t)$ |
| Model Parameters | $m_m=\varepsilon_p+\frac{m}{(1-\delta)(1-\varepsilon_{mf})}$<br>$N_k=\frac{K_t H_f}{U_o}$<br>$Pe_B=\frac{U_o H_f}{E_s(\varepsilon_{fe}/\varepsilon_{se}+m_m)}$ | $m_m=\varepsilon_p+\frac{m}{(1-\delta)(1-\varepsilon_{mf})}$<br>$N_k=\frac{K_t H_f}{U_o}$ |

**Table 2.** $\mu_1$ and $\sigma^2$ expressions for the models used in the present study.

| Models | (BVS) | (M-BVS) |
|---|---|---|
| | $\mu_1 = \frac{\varepsilon_b H_f}{U_o}\left[m_B(\phi-1)-1\right]$ | $\mu_1 = \frac{\varepsilon_b H_f}{U_o}\left[1+m_B(1-\phi)\right]$ |
| | $\sigma^2 = N^2\left\{\frac{2}{N_k}\left[\frac{(1-\phi)(m_B+1)}{N}\right]^2+\frac{2}{N_E}+\frac{2q}{N_E^2}\frac{\left(e^{0.5N_k(q-1)}-1\right)\left(e^{0.5N_k(q+1)}-1\right)}{e^{0.5}N_k^{(q-1)}-e^{-0.5}N_k(q+1)}\right\}$ | $\sigma^2 = \frac{2\left[(m_B+1)(1-\phi)\right]^2}{N_k}$ |
| **Models** | **(M)** | **(M–M)** |
| | $\mu_1 = \frac{H_f}{U_o}\left[1+(1-\delta)(\varepsilon_{fe}+m_m\varepsilon_{se})\right]$ | $\mu_1 = \frac{H_f}{U_o}\left[\delta+(1-\delta)(\varepsilon_{fe}+m_m\varepsilon_{se})\right]$ |
| | $\sigma^2 = \frac{2\varepsilon^2}{N_k}+\frac{2}{Pe_B}+\frac{2q'}{Pe_B^2}\frac{\left(e^{0.5N_k(q'-1)}-1\right)\left(e^{0.5N_k(q'+1)}-1\right)}{e^{0.5N_k(q'-1)}-e^{0.5N_k(q'+1)}}$ | $\sigma^2 = \frac{2\varepsilon^2}{N_k}$ |

mass transfer coefficient between bubble and emulsion phases ($K_{be}$) are related as:

$$\delta(K_{be})_b = a_b k_{be} = K_t \tag{11}$$

where ($K_t$) is the overall gas interchange coefficient based on the total volume of the bed.

Davidson and Harrison (1963) assumed that the transfer of gas between bubble and cloud is caused by a combination of convective through flow and molecular diffusion. They have derived the following expression for $(K_{bc})_b$ for a spherical bubble of diameter ($d_b$):

$$(K_{bc})_b = 4.5\frac{U_{mf}}{d_b}+5.85\left[\frac{D^{\frac{1}{2}}g^{\frac{1}{4}}}{d_b\,5/4}\right] \tag{12}$$

The transfer of gas between cloud and emulsion occurs primarily by diffusion. Applying Higbie's penetration model at the interphase, one can derive the gas interchange coefficient between cloud and emulsion, $(K_{ce})_b$ (Kunii and Levenspiel, 1968), as:

$$(K_{ce})_b = 6.78\left[\frac{\varepsilon_{mf}D_eU_b}{d_b^3}\right]^{\frac{1}{2}} \tag{13}$$

Drinkenburg and Rietema (1972) predicted the interphase transfer rate for isolated single two-dimensional bubbles and modified the overall mass transfer coefficient between bubble and emulsion phases, $k_{be}$, as:

$$k_{be} = \frac{3}{4}U_{mf}+\left(\frac{gD^2}{d_b}\right)^{\frac{1}{4}} \tag{14}$$

Sit and Grace (1981) suggested the following relation for the mass transfer coefficient between bubble and emulsion phases by taking into account the enhancement of mass transfer due to the bubble interaction in a freely bubbling bed:

$$k_{be} = \frac{U_{mf}}{4}+\left(\frac{4D\varepsilon_{mf}U_b}{\pi d_b}\right)^{\frac{1}{2}} \tag{15}$$

In Equations (12), (14) and (15) the first terms at the righthand side of the expressions are the convective terms. The second terms describe the effect of molecular diffusion according to the penetration theory. It is necessary to modify these expressions in the case of adsorption. Chiba and Kobayashi (1970) derived an expression for the ratio of the gas interchange coefficient in the presence of adsorption ($K_d$) to the coefficient in the absence of adsorption, $(K_{be})_b$, at incipient fluidization for a single bubble, as given below:

$$\frac{K_d}{(K_{be})_b} = \left[1+\frac{2}{3}m\left(\frac{1-\varepsilon_{mf}}{\varepsilon_{mf}}\right)\left(\frac{1}{2}+\frac{\alpha}{\alpha-1}\right)\right]^{\frac{1}{2}} \tag{16}$$

where $m$ is the adsorption equilibrium constant and $\alpha$ is defined as:

$$\alpha = \frac{U_b\varepsilon_{mf}}{U_{mf}} \tag{17}$$

The following four methods were used to estimate the gas interchange coefficients and were compared with the values obtained through second moment analysis of RTD for tracer gases. Method 1 involves the use of Equations (12) and (13) for the estimation of $(K_{bc})_b$ and $(K_{be})_b$, respectively. These values are substituted in Equation (7) to calculate $(K_{be})_b$. Equation (16)

was employed to calculate $K_d$ when the value of $(K_{be})_b$ was known. In Method 2, Equation (15) was used to estimate $K_{be}$. In Method 3, Equation (15) neglecting the diffusive term, was used. In Method 4, Equation (12) neglecting the diffusive term was used. Gas interchange coefficients are converted into $K_{be}$ using relations given in Equations (9) to (11).

## Experimental

### Apparatus

The experiments were performed in a system shown schematically in Figure 1. The fluidized bed reactor was a Pyrex column of 0.074 m inside diameter and 1 m in height. It was fitted with a perforated stainless steel gas distributor containing 90 holes each of which was 0.7 mm in diameter. A 250 mesh screen was placed just below the distributor plate. The column was wrapped by heating tape, and the temperature in the bed was measured by a Fe-constant thermocouple. The reactor was insulated by glass-wool lagging. The pressure just below the distributor was measured with a Datametrics electronic manometer and a pressure transducer.

Air, which was the main fluidizing gas, was supplied to the reactor by a compressor and dried in two dehumidifier columns filled with silica gel and Zeolite 5A particles. The air was preheated in an electrical furnace before being fed to the fluidized bed. A cyclone was placed at the top of the reactor to collect the entrained particles.

Tracer gas was injected into the column just below the distributor by using a sample valve with a sample loop of 1.5 ml. Concentration of tracer gas in the exit gas stream was measured by the flame ionization detector of a gas chromatograph (Packard Model 427). Sample gas was taken by using a copper tube of 1.6 mm inside diameter from just above the surface of the fluidized bed. The tip of the sampling tube was filled with quartz wool and covered with 250 mesh screen to prevent the particles entering the tube.

The analog signals obtained from the flame ionization detector, which is directly related to the concentration of tracer gas in the exit gas stream, were converted into digital signals with a multi-function data acquisition card (PCL 711) connected to a PC.

### Materials

A commercial Silica/Alumina Gel Based Zeolite Cracking Catalyst (CBZ-2) manufactured by Davison Company was used as fluidized particles in the experiments. The chemical analyses and the physical properties of the catalyst are given in Tables 3 and 4. Three different hydrocarbon gases were used as the adsorbable tracer gases in the experiments. These gases were methane, ethane, and propane, which were obtained from Matheson Company as chemically pure (CP) grade.

### Procedure

The system was operated in a semi-batch manner with a single initial input of particles. The bed was first loaded with an amount of catalyst particles to give a static bed height of 17.7 cm. The flow rate of air was set to the desired value, and after steady state temperature was reached in the bed, the tracer gas was injected into the column just below the distributor with the sample valve. In a set of runs the RTD curves were obtained for different air velocities at a given temperature and for a specific tracer gas. Experiments were performed over an air velocity range of 0.01 to 0.04 m/s and at temperatures between 323 and 435 K. The experiments were repeated several times to check the reproducibility.

After ten to twelve RTD experiments the CBZ-2 catalyst was regenerated. Regeneration was performed in the fluidized bed column. Temperature in the column was increased to around 473 K and it was fluidized by dehumidified air for about 6 h.

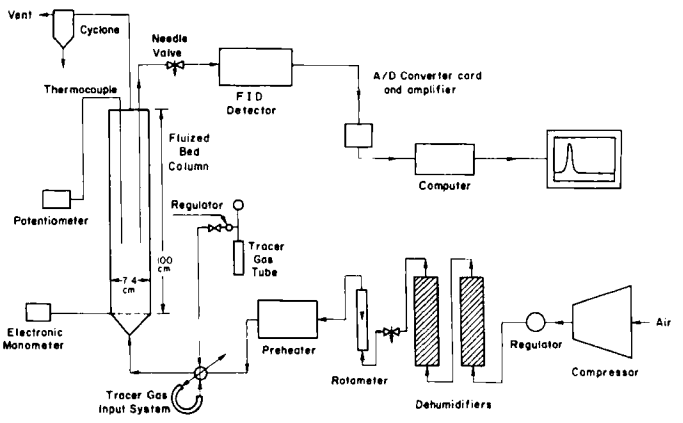


**Figure 1.** Schematic diagram of the experimental setup.

**Table 3.** Chemical analysis of CBZ-2.

| $Al_2O_3$ wt % DB | $Na_2O$ wt % DB | Fe wt % DB | V ppm DB | Ni ppm DB | Cu ppm DB |
|---|---|---|---|---|---|
| 33.0 | 0.50 | 0.33 | 615 | 175 | 11 |

**Table 4.** Physical properties of CBZ-2.

| | |
|---|---|
| $\rho_p$, kg/m$^3$ | 989.5 |
| $\rho_s$, kg/m$^3$ | 2484.3 |
| $\varepsilon_p$ | 0.6017 |
| $S_g$, m$^2$/kg | $2.078 \times 10^5$ |
| $V_{pore}$, m$^3$/kg | $6.08 \times 10^{-4}$ |
| zeolite content | 10% by XRD |

### *Data Analysis*

Response curves of tracer pulse inputs (RTD curves) were used to calculate the first absolute moment and the second central moment by using the following expressions:

$$\mu_1 = M_1/M_0 \tag{18}$$

$$\sigma^2 = M_2/M_0 - (M_1/M_0)^2 \tag{19}$$

where

$$M_n = \int_0^\infty t^n\, C(t)\, dt \tag{20}$$

$M_n$ was evaluated from the RTD curves by using Simpson's one-third rule for numerical integration.

$\mu_1$ and $\sigma^2$ values for the dead volumes (in the gas feeding, fluidized bed section, gas sampling and gas analysis systems) were evaluated from the empty column RTD curves. These values were subtracted from the $\mu_1$ and $\sigma^2$ values evaluated from the RTD curves obtained in the fluidized bed experiments in order to correct for the dead volume. These corrections were repeated for all the tracer gases and at different gas velocities.

The small values of the $\sigma^2/\mu_1^2$, which varied, in general, from 0.05 to 0.1, showed that the impulse in the reactor was very close to a perfect pulse.

Experimental $\mu_1$ and $\sigma^2$ data were compared with theoretical $\mu_1$ and $\sigma^2$ expressions of the four different models to evaluate model parameters. A non-linear regression method was utilized for this comparison (Marquardt, 1963).

### *Determination of Adsorption Equilibrium Constants by the Gas Chromatography Technique*

The adsorption equilibrium constants, *m*, of the tracer gases at different temperatures were measured by using the gas chromatography technique as explained by Schneider and Smith (1968). The basic principle of this technique can be explained as follows: The chromatographic curves of the effluent from a fixed bed of catalyst particles obtained by injecting a pulse of tracer gases in a carrier gas stream can be used to evaluate the first absolute moment values of the RTD curves. Values of $\mu_1$ obtained at different superficial carrier gas velocities were used to evaluate the adsorption equilibrium constant, *m*, by comparing these data with the theoretical $\mu_1$ expression given by Schneider and Smith (1968). *m* was defined as the ratio of concentration of gas on particle surface per unit volume of gas in the interparticle space to the concentration of adsorbable gas in the interparticle space.

Hewlett-Packard 5890 II gas chromatograph with a flame ionization detector was used to measure the response curves of tracer gases on a fixed bed of CBZ-2 catalyst particles of 0.42 cm i.d., 18 cm packed length. Nitrogen was used as the carrier gas. The amount of adsorbable gases injected into the system was kept constant at 0.025 $cm^3$ to keep the concentration of adsorbable gases very low. This fulfilled the assumption of linear adsorption isotherm. The first absolute moments of the RTD curves were evaluated by using the response curves obtained from the flame ionization detector in terms of electrical signals, following the same procedure used in fluidized bed experiments, as explained above.

## Results and Discussion

The expressions for $\mu_1$ and $\sigma^2$ are given in Table 2 for four dynamic fluidized bed reactor (FBR) models considered in this work. In these models, ($m_B$) and ($m_m$) are the only model parameters that are to be determined from the first moment data, whereas ($K_t$) is estimated from variance data. All the other parameters are evaluated from the well known hydrodynamic relations given in the literature for FBR, listed in Table 5.

### The Adsorption Equilibrium Constant

The adsorption equilibrium constant calculated from the first moment data of RTDs for the three tracer gases methane, ethane and propane are given in Table 6. All four models gave essentially the same values and thus could be shown in a single column in Table 6. There is also a remarkable agreement between these values and those determined by gas chromatographic measurements. This is particularly true for methane and ethane tracer gases. For propane at the lowest temperature (338 K), values of the adsorption equilibrium constants determined by fluidized bed and chromatographic experiments differ slightly. This may be attributed to the departure from linearity obtained in the fixed bed experiments. Nonlinear adsorption is expected to be less pronounced in the fluidized bed experiments because of the dilution of the tracer gas with the large amount of fluidizing air.

Since fluidized bed and fixed bed experiments gave essentially identical adsorption equilibrium constants for tracer gases, van't Hoff plots of the adsorption equilibrium constants evaluated by both experiments are plotted together in Figure 2. Expected linear dependence of the logarithm of the equilibrium constant (*m*) on reciprocal temperature can be considered as further evidence of the physical significance of the constants evaluated from the models.

From van't Hoff plots limiting the heat of adsorption for methane, ethane and propane on the CBZ-2 catalyst was found to be 9.94, 15.98 and 24.28 kJ/mol, respectively. Schneider and Smith (1968) reported heats of adsorption of ethane and propane on a commercial silica alumina cracking catalyst as being 17.15 and 23.85 kJ/mol, which were close to the values reported in this study.

### Mass Transfer Coefficients

Overall mass transfer coefficients, $K_t$, calculated from the best fit of all four models and $\sigma^2$ data of RTD's for tracer gases methane, ethane, and propane are shown in Figures 3 to 5. Since BVS and M models and similarly M-BVS and M-M models gave essentially the same values of $K_t$, each pair is represented by the same symbol in order not to clutter the figures.

It is interesting to note that modified models, although simpler, give very close values (within 2%) to those of the original models. These results support the claims by Grace (1985) and Uysal et al. (1988) that even the simplest two-phase model assuming a stationary emulsion phase predicts the fluidized bed performance quite satisfactorily. Figures 3 to 5 indicate that $K_t$ increases as flow rate increases for all tracer gases at all temperatures. $K_t$ appears to decrease as temperature increases. This is more pronounced for propane gas which has a larger adsorption equilibrium constant than methane and ethane.

Figure 6 shows the effect of the adsorption equilibrium constant on the gas interchange coefficient at constant superficial velocities for different tracer gases. Figure 6 indicates that when the adsorption equilibrium constant is relatively small the gas interchange coefficient can be considered as constant. However, at larger values of *m*, $K_t$ becomes larger. This effect becomes more pronounced at relatively large values of $U_o$.

Morooka et al. (1977) studied the effect of gas adsorption on the mass transfer between bubbles and emulsion phase by measuring the residence time distributions of tracer gases helium, carbon dioxide, Freon 12, and Freon 22 in 12 and 15 cm diameter free and baffled beds of cracking catalyst. They reported that the gas interchange coefficients expressed as $k_{ob}a_b/\varepsilon_b$ approach a constant value for $m < 1$ or $m > 100$. The coefficient become larger with increasing *m* for $1 < m < 100$. The results of this study are consistent with their conclusions.

An empirical relation for the gas interchange coefficient between the bubble and emulsion phases as a function of *m* and $U_o$ is obtained by using data in Figure 6. The best fit gives the following empirical relation:

**Table 5.** Hydrodynamic parameters for FBR.

| Parameter | Relation | Reference |
|---|---|---|
| Minimum fluidization velocity | $U_{mf} = 1.1\times10^{-3}\dfrac{(d_p)^{1.82}(\rho_p-\rho_g)^{0.94}(g)^{0.94}}{(\rho_g)^{0.06}(\mu_g)^{0.88}}$ (Leva's Correlation) | (Yates, 1983) |
| Average bubble diameter | $d_b = \dfrac{1.30}{g^{0.2}}\left[\dfrac{U_o - U_{mf}}{N_{or}}\right]^{0.4}$ and $d_{bmax}$ | (Davidson and Harrison, 1963)<br>(Kunii and Levenspiel, 1969) |
| Height of fluidized bed | $\dfrac{H_f}{H_{mf}} = 1+\dfrac{U_o - U_{mf}}{0.711(gd_b)^{1/2}}$ | (Kunii and Levenspiel, 1969) |
| Fraction of fluidized bed occupied by bubble | $\delta = \dfrac{H_f - H_{mf}}{H_f}$ | |
| Interfacial area per bubble volume | $a = 6/d_b$ | |
| Axial dispersion coefficient | $\dfrac{E_s}{\{g(U_o-U_{mf})\}^{1/3}D_{bed}^{4/3}} = 1.058\left[\dfrac{\mu_g}{18U_T d_p \rho_g}\right]^{0.368}$<br>where<br>$U_T = \dfrac{g d_p^{\,2}(\rho_s-\rho_g)}{18\mu_g}$ $\quad Re_t < 1$ | (Lee et al., 1991) |

**Table 6.** Adsorption equilibrium constants (m) evaluated from gas chromatography (GC) and fluidized bed (FB) experiments.

| Gas | Temperature, K | GC | FB |
|---|---|---|---|
| Methane | 326 | 0.39 | 0.39 |
| | 363 | 0.26 | 0.27 |
| | 418 | 0.17 | 0.18 |
| Ethane | 323 | 1.42 | 1.37 |
| | 368 | 0.68 | 0.69 |
| | 423 | 0.35 | 0.36 |
| Propane | 338 | 5.48 | 6.49 |
| | 383 | 1.98 | 2.07 |
| | 435 | 0.79 | 0.81 |

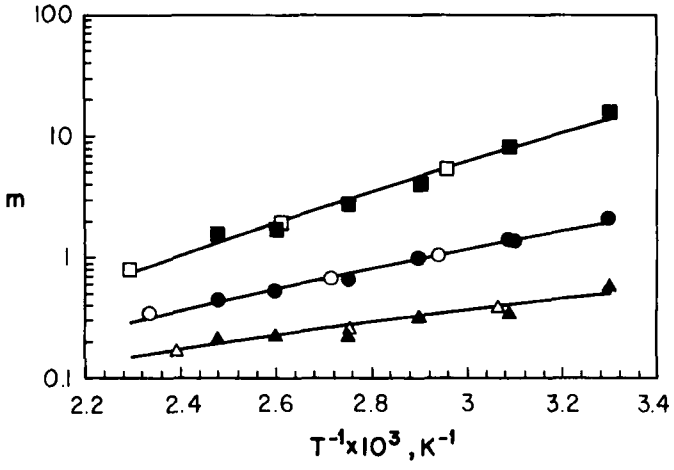


**Figure 2.** Van't Hoff Plots of the adsorption equilibrium constant ($m$). △: methane; ○: ethane; □: propane. Open and filled symbols denote values obtained by fluidized and gas chromatography experiments, respectively.

$$K_t = 1.518U_o^{0.88}\ \exp(0.158\ m) \qquad (21)$$

It should be mentioned that Equation (21) may only be applicable to fluidized beds that are very similar to the test unit in the present work, since $K_t$ is known to depend on other parameters as well, such as bubble diameter, which in turn is influenced by the size of the fluidized bed. In the present study $m$ varies between 0.2 and 6.5, and $U_o/U_m$ varies between 5 and 30. Morooka et al. (1977) have proposed an empirical equation where $1 < m < 30$ and $60 \le u_o / u_{mf} \le 300$:

$$\frac{K_t}{\varepsilon_b} = \left(15m^{1.8}+229\right)/\left(m^{1.8}+191\right) \qquad (22)$$

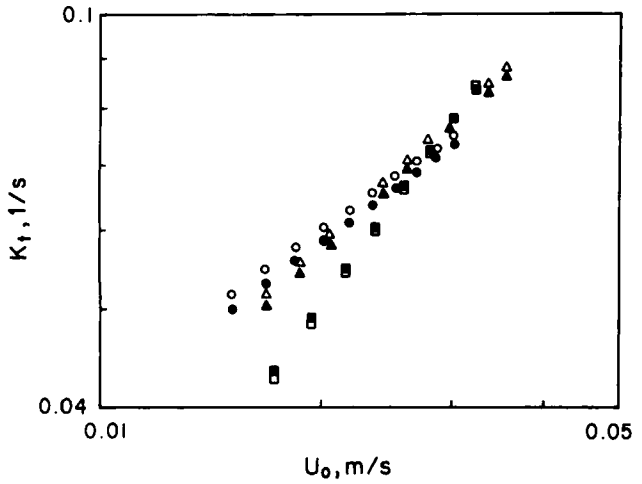


**Figure 3.** The overall gas interchange coefficient for methane as function of superficial velocity and temperatures. ○: 328 K; △: 363 K; □: 418 K. Open symbols denote BVS or M models and filled symbols M-BVS or M-M models.

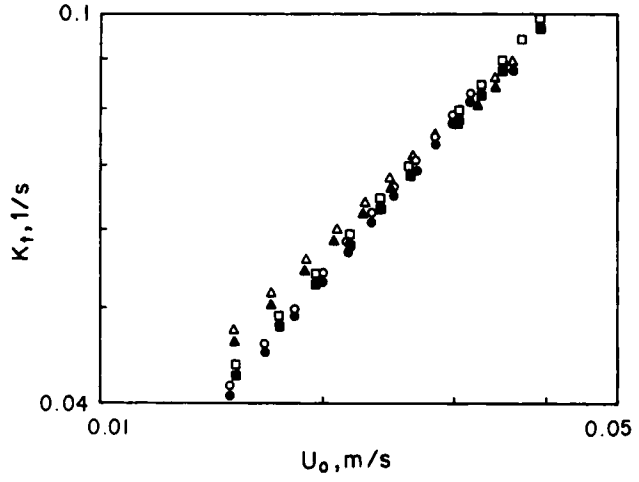


**Figure 4.** The overall gas interchange coefficients for ethane as a function of superficial velocity and temperatures. ○: 323 K; △: 363 K; □: 423 K. Open symbols denote BVS or M models and filled symbols M-BVS or M-M models.

$\varepsilon_b$ values in the present study were around 0.8. The two equations, Equation (21) and Equation (22), are shown for comparison in Figure 7. It is interesting to note that Morooka's equation, Equation (22), does not depend on $U_0$, and the extrapolation of the present correlation Equation (21) coincides with their correlation for $U_0$ values greater than 0.5 m/s.

In our study, the velocities had to be kept low in order to minimize the elutriation of finer particles, which is known to alter the fluidizing characteristics drastically for A type particles like FCC catalysts. Obviously, data over a larger velocity range are needed for different systems to draw firmer conclusions.

Figures 8 and 9 show experimental $k_{be}$ values obtained by the application of BVS model to $\sigma^2$ data of RTD for propane at two different temperatures together with the values estimated by the four methods described previously. The results obtained for methane and ethane at different temperatures have similar trends. It is observed that Methods 1 and 2 give significantly

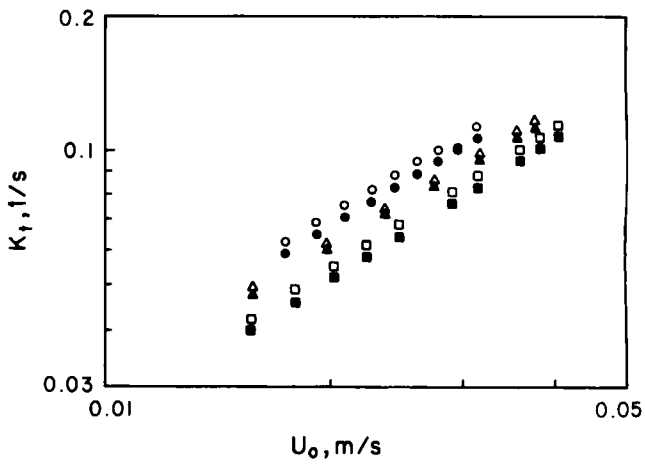


**Figure 5.** The overall gas interchange coefficients for propane as a function of superficial velocity and temperatures. ○: 338 K; △: 383 K; □: 435 K. Open symbols denote BVS or M models and filled symbols M-BVS or M-M models.

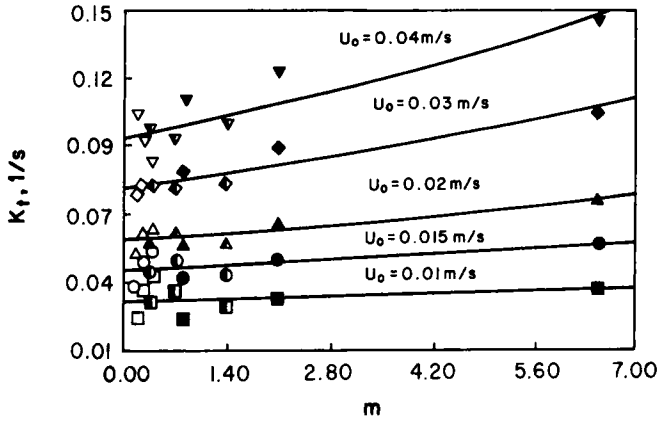


**Figure 6.** The overall gas interchange coefficients as a function of the adsorption equilibrium constants and superficial velocities. Empty symbols denote methane, half-filled symbols ethane and filled symbols propane.

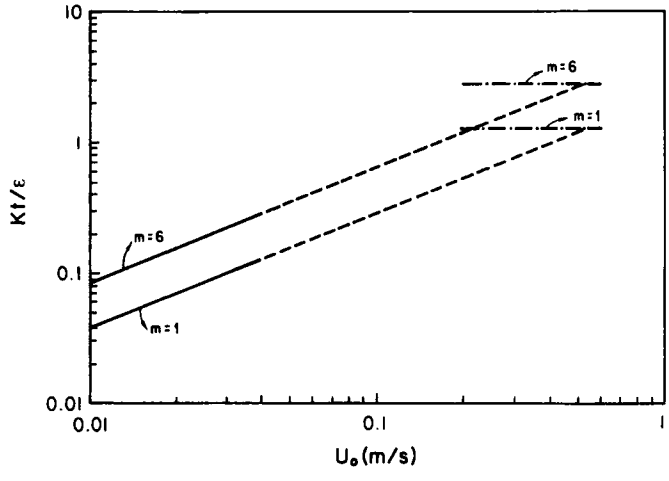


**Figure 7.** The comparison of correlation for the bubble-emulsion transfer coefficient, $k_t/\varepsilon_b$ obtained in this work, Equation (21), and that of Morooka et al. (1971) Equation (22).

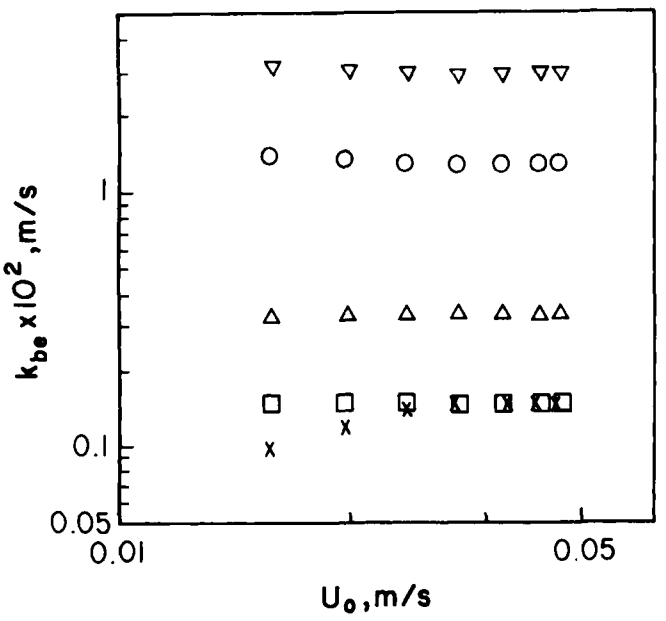


**Figure 8.** The bubble-emulsion transfer coefficient, $k_{be}$, obtained by RTD using the BVS model and estimated from correlations for propane. The temperature is 383 K. 0 method 1; ∇ method 2; Δ method 3; x: method 4; x: model.

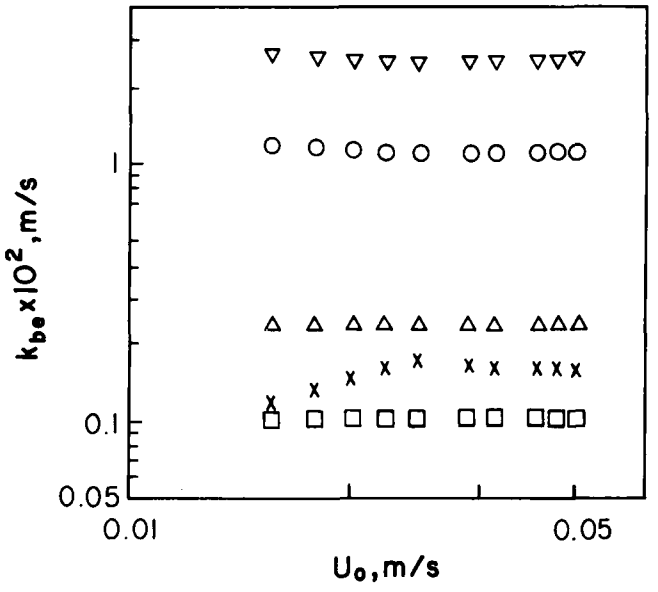


**Figure 9.** The bubble-emulsion transfer coefficient, $k_{be}$ obtained by RTD using the BVS model and estimated from correlations for propane. Temperature is 435 K. 0 method 1; ∇ method 2; Δ method 3; x: method 4; x: model.

larger values than the experimental results, whereas Methods 3 and 4 give relatively closer values to the experimental ones. The basic difference between these methods is that the former methods include diffusional flux in addition to the convective flux. It appears that diffusion plays an insignificant role on mass transfer for adsorbing species in fluidized bed reactors. A similar conclusion was reached by Bohle and van Swaaij (1978) in their studies involving nonadsorbing and absorbing species with a commercial cracking catalyst. They observed that the gas interchange coefficients of helium and argon were too close to each other in spite of a large difference between their diffusivities and concluded that the mass transfer coefficient between the phases does not depend on molecular diffusivities.

The dependency of experimental $k_{be}$ on superficial gas velocity is much more pronounced than the estimated $k_{be}$ values. In general, experimental $k_{be}$ values lie in between values evaluated by Methods 3 and 4. The values obtained at low $U_0$ are close to the results of Method 3, whereas at higher $U_0$ Method 4 gives closer values.

## Conclusions

RTDs of tracer gases methane, ethane and propane on a commercial FCC catalyst using an air fluidized laboratory scale reactor were determined over a superficial velocity and temperature range.

The adsorption equilibrium constants evaluated by the best fit of four dynamic models and those constants determined from GC experiments were very close.

The gas interchange coefficients between the bubble and emulsion phases evaluated by second moment analysis of the four models gave very similar values and were shown to increase with an increase in adsorption equilibrium constant and superficial velocity. Gas interchange coefficients estimated from the methods available in the literature indicated that if diffusive fluxes were neglected in favour of convective fluxes, their values are closer to the experimental measurements. However, it has been found that none of the methods present in the literature is adequate to express the influence of air velocity on mass transfer. Consequently, an empirical relation (Equation 21) which takes into account air velocity and the adsorption equilibrium constant, is proposed.

However, we caution that this equation can be used only for a similar sized fluidized bed and the range of conditions employed in the present study.

## Appendix

We outline here the derivation of Bohle and van Swaaij (BVS) model that leads to the expressions for the first and second absolute moments given in Table 2. Derivations of other methods are quite similar.

Taking Laplace transformations of the dimensionless transient conservation of mass equations and the initial and boundary conditions given for the BVS model in Table 1, one obtains:

$$\phi p \bar{C}_b + \frac{d\bar{C}_b}{d\zeta} + N_k\left(\bar{C}_b - \bar{C}_e\right) = 0 \tag{A1}$$

$$\left(m_B + 1\right)(1-\phi)p\,\bar{C}_e - \frac{1}{N_E}\frac{d^2\bar{C}_e}{d\zeta^2} - N_k\left(\bar{C}_b - \bar{C}_e\right) = 0 \tag{A2}$$

$$\zeta = 0 \qquad \bar{C}_b = 1 \qquad \frac{d\bar{C}_e}{d\zeta} = 0 \tag{A3}$$

$$\zeta = 1 \qquad \frac{d\bar{C}_e}{d\zeta} = 0 \tag{A4}$$

From Equations (A1) and (A2), the following characteristics equation is obtained:

$$\lambda^3 - \lambda^2(-\phi p + N_k) - \lambda\left[(m_B+1)(1-\phi)pN_E + N_E N_k\right]$$
$$-\left[(m_B+1)(1-\phi)p(\phi p + N_k)N_E + (\phi p N_E N_k)\right] = 0 \quad \text{(A5)}$$

The roots of Equation (A5) are related as follows:

$$\lambda_1 + \lambda_2 + \lambda_3 = -\phi p - N_k \quad \text{(A6)}$$

$$\lambda_1\lambda_2 + \lambda_1\lambda_3 + \lambda_2\lambda_3 = -(1-\phi)(m_B+1)\,pN_E - N_E N_K \quad \text{(A7)}$$

$$\lambda_1\lambda_2\,\lambda_3 = (1-\phi)(m_B+1)p(\phi p + N_k)\,N_E + \phi p N_E N_K \quad \text{(A8)}$$

Laplace domain solutions of $\bar{C}_b(\zeta,p)$ and $\bar{C}_e(\zeta,p)$ are:

$$\bar{C}_b = a_1 e^{\lambda}1^{\zeta} + a_2 e^{\lambda}2^{\zeta} + a_3 e^{\lambda}3^{\zeta} \quad \text{(A9)}$$

$$\bar{C}_e = b_1 e^{\lambda}1^{\zeta} + b_2 e^{\lambda}2^{\zeta} + b_3 e^{\lambda}3^{\zeta} \quad \text{(A10)}$$

where

$$a_1 = \frac{x_2x_3\left(e^{\lambda}3 - e^{\lambda}2\right)}{x_2x_3\left(e^{\lambda}3 - e^{\lambda}2\right) + x_1x_3\left(e^{\lambda}1 - e^{\lambda}3\right) + x_1x_2\left(e^{\lambda}2 - e^{\lambda}1\right)} \quad \text{(A11)}$$

$$a_2 = \frac{x_1x_3\left(e^{\lambda}1 - e^{\lambda}2\right)}{x_2x_3\left(e^{\lambda}3 - e^{\lambda}2\right) + x_1x_3\left(e^{\lambda}1 - e^{\lambda}3\right) + x_1x_2\left(e^{\lambda}2 - e^{\lambda}1\right)} \quad \text{(A12)}$$

$$a_3 = \frac{x_1x_2\left(e^{\lambda}2 - e^{\lambda}1\right)}{x_2x_3\left(e^{\lambda}3 - e^{\lambda}2\right) + x_1x_3\left(e^{\lambda}1 - e^{\lambda}3\right) + x_1x_2\left(e^{\lambda}2 - e^{\lambda}1\right)} \quad \text{(A13)}$$

$$b_i = a_i y_i \quad \text{(A14)}$$

$$y_i = \frac{\phi p + \lambda_i + N_k}{N_k} \quad \text{(A15)}$$

$$x_i = y_i\lambda_i \quad \text{(A16)}$$

At the exit of the bed $\zeta = 1$, $\bar{C}b$ and $\bar{C}e$ are:

$$\bar{C}_{b_{\zeta=1}} = \frac{\alpha_1 e^{\lambda}1 + \alpha_2 e^{\lambda}2 + \alpha_3 e^{\lambda}3}{\alpha_1 + \alpha_2 + \alpha_3} \quad \text{(A17)}$$

$$C_{e_{\zeta=1}} = \frac{x_1x_2x_3}{x_2x_3\left(e^{\lambda}3 - e^{\lambda}2\right) + x_1x_3\left(e^{\lambda}1 - e^{\lambda}3\right) + x_1x_2\left(e^{\lambda}2 - e^{\lambda}1\right)}$$
$$\left[\frac{e^{\lambda}1}{\lambda 1} + \frac{e^{\lambda}2}{\lambda 2} + \frac{e^{\lambda}3}{\lambda 3}\right] \quad \text{(A18)}$$

where

$$\alpha_1 = \frac{e^{\lambda}3 - e^{\lambda}2}{\phi p + \lambda_1 + N_k} \quad \text{(A19)}$$

$$\alpha_2 = \frac{\lambda_1}{\lambda_2}\frac{e^{\lambda}1 - e^{\lambda}3}{\phi p + \lambda_2 + N_k} \quad \text{(A20)}$$

$$\alpha_3 = \frac{\lambda_1}{\lambda_3}\frac{e^{\lambda}2 - e^{\lambda}1}{\phi p + \lambda_3 + N_k} \quad \text{(A21)}$$

The limits of Equations (A17) and (A18) as the Laplace parameter $p$ approaches zero give the zeroth moment expressions or the steady state solutions of $\bar{C}_b$ and $\bar{C}_e$ at the exit. The zeroth moment of $\bar{C}_b$ is expressed as follows :

$$M_o = \lim_{p \Rightarrow o} \bar{C}_b(\zeta,p)_{\zeta=1} = \frac{\alpha_{10}e^{\lambda}10 + \alpha_{20}e^{\lambda}20 + \alpha_{30}e^{\lambda}30}{\alpha_{10} + \alpha_{20} + \alpha_{30}} \quad \text{(A22)}$$

$\lambda_{10}$, $\lambda_{20}$ and $\lambda_{30}$ are the roots of the equations obtained from Equation (A5) when $p \Rightarrow 0$:

$$\lambda_{10} = 0 \quad \text{(A23)}$$

$$\lambda_{20} = \frac{q-1}{2}N_k \quad \text{(A24)}$$

$$\lambda_{30} = -\frac{q+1}{2}N_k \quad \text{(A25)}$$

where

$$q = \sqrt{1 + 4(N_E / N_k)} \quad \text{(A26)}$$

Therefore, the zeroth moment of the RTD function at the exit of the bed is obtained as:

$$M_o = \lim_{p \Rightarrow o} \bar{C}_{b_{\zeta=1}} = e^{\lambda}10 = 1 \quad \text{(A27)}$$

The first moment of the RTD function is the mean residence time of the bubble phase, which is defined as the following:

$$M_1 = \lim_{p \Rightarrow o} \frac{\partial\bar{C}(\zeta,p)}{\partial p}_{\zeta=1} = \lim_{p \Rightarrow o} \bar{C}'_{b_{\zeta=1}} \quad \text{(A28)}$$

Differentiation of Equation (A17) gives:

$$\bar{C}'_{b\,\zeta=1}\sum\alpha_i + \bar{C}_{b\,\zeta=1}\sum\alpha'_i = \sum\alpha'_i\,e^{\lambda}i + \sum\alpha_i\lambda'_i\,e^{\lambda}i \quad \text{(A29)}$$

$$\lim_{p \Rightarrow o} \bar{C}_{b'_{\zeta=1}} = \frac{\alpha'_{20}}{\alpha_{10}}\left(e^{\lambda}20 - 1\right) + \frac{\alpha'_{30}}{\alpha_{10}}\left(e^{\lambda}30 - 1\right) + \lambda'_{10} \quad \text{(A30)}$$

$\lambda'_{10}$ is derived by differentiating Equation (A8) with respect to $p$ and by taking the limit as $p \Rightarrow 0$:

$$\lambda'_{10} = -[1 + m_B(1 - \phi)] \tag{A33}$$

The first moment expression is obtained as:

$$M_1 = \lambda'_{10} = 1 + m_B(1 - \phi) \tag{A34}$$

The second moment of the RTD function is defined as:

$$M_2 = \lim_{p \Rightarrow o} \left.\frac{\partial^2 \bar{C}(\zeta, p)}{\partial p^2}\right|_{\zeta=1} = \lim_{p \Rightarrow o} \bar{C}''_{b\,\zeta=1} \tag{A35}$$

Differentiation of Equation (A28) yields:

$$\begin{aligned} &\bar{C}''_{b\,\zeta=1} \sum \alpha_i + 2\bar{C}'_{b\,\zeta=1} \sum \alpha'_i + \bar{C}_{b\,\zeta=1} \sum \alpha''_i \\ &= \sum \alpha''_i e^{\lambda}{}_i + 2\sum \alpha'_i \lambda'_i e^{\lambda}{}_i \\ &+ \sum \alpha_i \lambda''_i e^{\lambda}{}_i + \sum \alpha_i (\lambda'_i) 2 e^{\lambda}{}_i \end{aligned} \tag{A36}$$

when $p \Rightarrow$ O:

$$\lim_{p \Rightarrow o} \bar{C}''_{b\,\zeta=1}\, \alpha_{10} = \frac{2\lambda'_{10}\left(e^{\lambda}20 - 1\right)\left(e^{\lambda}30 - 1\right)}{N_E{}^2 N_k{}^2}$$

$$(\lambda_{30} - \lambda_{20})(-\phi - \lambda'_{20} - \lambda'_{30}) + \alpha_{10}\left(\lambda''_{10} + (\lambda''_{10})^2\right) \tag{A37}$$

where

$$(\lambda'_{20} + \lambda'_{30}) = -\phi - \lambda'_{10} \tag{A38}$$

$$\lambda''_{10} = (1 - \phi)(m_B + 1)\left[\frac{2\lambda'_{10}}{N_k} - \frac{2\phi}{N_k}\right] + \frac{2(\lambda'_{10})^2}{N_E} \tag{A39}$$

Finally, the second moment is derived as follows:

$$\begin{aligned} M_2 = &\frac{2(-\lambda'_{10})^2\left(e^{\lambda}20 - 1\right)\left(e^{\lambda}30 - 1\right)}{\left(e^{\lambda}20\right) - \left(e^{\lambda}30\right) N_E{}^2} q(-\lambda'_{10})^2) \\ &+ \frac{2(1-\phi)(m_B + 1)}{N_k}\left[-(\lambda'_{10} + \phi)\right] + \frac{2(-\lambda'_{10})^2}{N_E} \end{aligned} \tag{A40}$$

Substituting Equations (A27), (A34) and (A40) into Equations (18) and (20), one obtains the expressions for the first absolute moment and second central moment for the Bohle and van Swaaij model (BVS) given in Table 2.


## Acknowledgements

This research was funded by METU Project Fund as AFP 90-03-04-02 and TUBITAK as Project No. MISAG-A-18.


## Nomenclature

| | |
|---|---|
| $a$ | interfacial area per unit bubble volume, ($ms^{-1}$) |
| $a_b$ | interfacial area per bed volume, ($ms^{-1}$) |
| $C_b$ | concentration of the adsorbing gas in the bubble phase, ($mol/m^3$) |
| $C_c$ | concentration of the adsorbing gas in a cloud, ($mol/m^3$) |
| $C_e$ | concentration of the adsorbing gas in the emulsion phase, ($mol/m^3$) |
| $d_b$ | average bubble diameter, (m) |
| $d_{b\,max}$ | maximum stable bubble diameter, (m) |
| $d_p$ | average particle diameter, (m) |
| $D$ | diffusivity of adsorbing gas, ($m^2/s$) |
| $De$ | effective diffusivity of adsorbing gas in the emulsion phase, ($m^2/s$) |
| $D_{bed}$ | diameter of the fluidized bed, (m) |
| $E_e$ | overall axial dispersion coefficient for the adsorbing gas in the emulsion phase based on a cross sectional area of the empty column, ($m^2/s$) |
| $E_{fe}$ | apparent axial dispersion coefficient of the adsorbing gas in the emulsion phase, ($m^2/s$) |
| $E_g$ | axial dispersion coefficient of the adsorbing gas in the emulsion phase, ($m^2/s$) |
| $E_s$ | axial dispersion coefficient of solid particles in the emulsion phase, ($m^2/s$) |
| $E_{se}$ | apparent axial dispersion coefficient of the solid particles in the emulsion phase, ($m^2/s$) |
| $g$ | acceleration of gravity, ($m/s^2$) |
| $H_f$ | height of fluidized bed, (m) |
| $H_{mf}$ | height of bed at minimum fluidization, (m) |
| $k_{be}$ | overall mass transfer coefficient between bubble and emulsion phases, (m/s) |
| $(K_{bc})_b$ | gas interchange coefficient based on bubble volume at the bubble cloud interphase, (1/s) |
| $(K_{be})_b$ | overall gas interchange coefficient based on the bubble volume between bubble and emulsion phases, (1/s) |
| $(K_{ce})_b$ | gas interchange coefficient based on the bubble volume at the cloud emulsion interphase, (1/s) |
| $K_d$ | overall gas interchange coefficient based on bubble volume between the bubble and emulsion phase in the presence of adsorption effects, (1/s) |
| $K_t$ | overall gas interchange coefficient based on total volume of bed between the bubble and emulsion phases, (1/s) |
| $m$ | adsorption equilibrium constant |
| $m_B$ | adsorption equilibrium constant defined by Equation (1) |
| $m_m$ | adsorption equilibrium constant defined by Equation (3) |
| $m_n$ | $n^{th}$ moment. |
| $N$ | mean dimensionless residence time, $[1+m(1-ø)]$ |
| $N_a$ | number of moles of adsorbing gas, (moles) |
| $N_b$ | number of moles of adsorbing gas, in the bubble phase, (moles) |
| $N_k$ | number of transfer units, $K_t H_f / U_o$ |
| $N_E$ | number of axial dispersion units, $U_o H_f / [(m_B + 1)(1 - \delta) E_s]$ |
| $N_{or}$ | number of orificies per unit area of distributor, ($1/m^2$) |
| $Pe_B$ | number of axial dispersion units, $U_o H_f / (E_{fe} + m_m E_{se})$ |
| $Re_t$ | particle Reynold's number at terminal velocity, $(u_t d_p \rho_g)/\mu$ |
| $q$ | coefficient in Table 1, $\sqrt{1 + 4(N_E / N_k)}$ |
| $q'$ | coefficient in Table 1, $\sqrt{1 + 4(Pe_B / N_k)}$ |
| $\bar{r}$ | average pore radius of particles, (m) |
| $S_{be}$ | interfacial area between bubble and emulsion phases, ($m^2$) |
| $S_g$ | surface area of the particles, ($m^2/kg$) |
| $t$ | time, (s) |
| $U_b$ | bubble rise velocity with respect to stationary coordinate system, (m/s) |
| $U_{mf}$ | minimum fluidization velocity, (m/s) |
| $U_o$ | superficial velocity, (m/s) |

$U_T$ terminal velocity of the particles defined by Equation (8), (m/s)
$V_b$ bubble volume, ($m^3$)
$V_{pore}$ pore volume of particles, ($m^3$)
$z$ axial direction, (m)

### *Greek Symbols*

$\alpha$ ratio of bubble velocity to interstitial gas velocity, $U_{b\varepsilon_{mf}}/U_{mf}$
$\delta$ fraction of fluidized bed occupied by bubbles
$\delta(t)$ impulse function, ($mol/m^3$)
$\varepsilon$ coefficient defined in Table 1
$\varepsilon_b$ total porosity of fluidized bed, including particles' void fraction
$\varepsilon_{fe}$ voidage in emulsion phase
$\varepsilon_{mf}$ minimum fluidization voidage
$\varepsilon_p$ porosity of particles
$\varepsilon_{se}$ $(1 - \varepsilon_{fe})$
$\zeta$ dimensionless length, $z/H_f$
$\theta$ dimensionless time, $tU_o/\varepsilon_b H_f$
$\theta'$ dimensionless time, $tU_o/H_f[\delta + (1 - \delta)(\varepsilon_{fe} + m_m\varepsilon_{se})]$
$\mu_g$ viscosity of gas, (kg/m-s)
$\mu_1$ first absolute moment, (s)
$\rho_b$ bulk density, ($kg/m^3$)
$\rho_g$ gas density, ($kg/m^3$)
$\rho_p$ particle density, ($kg/m^3$)
$\rho_s$ solid density, ($kg/m^3$)
$\sigma^2$ second central moment, ($s^2$)
$\phi$ $\delta/\varepsilon_b$

## References


Akşahin, İ., "A Study of Dynamic Behavior of Catalytic Fluidized Bed Reactors", PhD Thesis, Middle East Technical University, Ankara, Turkey (1993).

Bohle, W. and W.P.M. van Swaaij, "The Influence of Gas Adsorption on Mass Transfer and Gas Mixing in a Fluidized Bed", in "Fluidization", J.F. Davidson and D.L. Keairns, Eds., Cambridge University Press, London, UK (1978), pp. 167–172.

Chiba, T. and H. Kobayashi, "Gas Exchange Between the Bubble and Emulsion Phases in Gas–Solid Fluidized Beds", Chem. Eng. Sci. **25**, 1375–1385 (1970).

Clift R., "Hydrodynamics of Bubbling Fluidized Beds" Chapter 4 in "Gas Fluidization Technology", D. Geldart, Ed., John Wiley & Sons Ltd., New York, NY (1986).

Davidson, J.F. and D. Harrison, "Fluidized Particles", Cambridge University Press, London, UK (1963).

Drinkenburg, A.A.H. and K. Rietema, "Gas Transfer From Bubbles in a Fluidized Bed to the Dense Phase – I. Theory", Chem. Eng. Sci. **27**, 1765–1774 (1972).

Drinkenburg, A.A.H. and K. Rietema, "Gas Transfer From Bubble in a Fluidized Bed to the Dense Phase – II. Experiments", Chem. Eng. Sci. **28**, 259–273 (1973).

Fane, A.G. and C.Y. Wen, "Fluidized Bed Reactors", in "Handbook of Multiphase Systems", G. Hetsroni, Ed., Hemisphere, Washington, DC (1982).

Grace, J.R. "Modelling and Simulation of Two-Phase Fluidized Bed Reactors" in "Proc. NATO-ASI", London, ON (1985).

Grace, J.R. "Fluid Beds as Chemical Reactors" in "Gas Fluidization Technology", D. Geldard, Ed., John Wiley & Sons Ltd., New York, NY (1986), pp. 287–341.

Hatano, H. and M. Ishida, "Interphase Mass Transfer *with Adsorption* and Chemical Reaction in a Fluidized Bed", Intern. Chem. Eng. **30**, 712–719 (1990)

Krambeck, F.J., A.A. Avidan, C.K. Lee, and M.N. Lo, "Predicting Fluidized-Bed Reactor Efficiency using Adsorbing Gas Tracers", AIChE J. **33**, 1727–1734 (1987).

Kunii, D. and O. Levenspiel, "Bubbling Bed Model for Kinetic Processes in Fluidized Beds", Ind. Eng. Chem. Process Des. Dev. **7**, 481–492 (1968).

Kunii, D. and O. Levenspiel, "Fluidization Engineering", Wiley, New York, NY (1969).

Kunii, D. and O. Levenspiel, "Phase Interchange Coefficients in Bubbling Fluidized Beds", J. Chem. Eng. Japan. **24**, 138–140 (1990).

Kühne, J. and D. Wippern, "Application of a Linear-Three-Phase Model to a Fluidized Bed Reactor", Can. J. Chem. Eng. **58**, 527–530 (1980).

Lee, G.S., S.D. Kim, and M.H.I. Baird, "Axial Mixing of Fine Particles in Fluidized Beds", Chem. Eng. J. **47**, 47–50 (1991).

Marquardt, D.W. "An Algorithm for Least Squares Estimation of Nonlinear Parameters", J. Soc. for Ind. and Appl. Math. **2**, 31–441 (1963).

May, W.G. "Fluidized-Bed Reactor Studies", Chem. Eng. Progr. **55**, 47–56 (1959).

Miyauchi, T.H. Kaji, and K. Saito, "Fluid and Particle Dispersion in Fluid-Bed Reactors", J. Chem. Eng. Japan **1**, 72–77 (1968).

Morooka, S.Y., Kato, and T. Miyauchi, "Hold-Up of Gas Bubbles and Longitudinal Dispersion Coefficient of Solid Particles in Fluid Bed Contactors for Gas–Solid Systems", J. Chem. Eng. Japan **5**, 161–167 (1972).

Morooka, S., M. Nishniaka, and Y. Kato, "Overall Mass Transfer Coefficient Between the Bubble Phase in Free and Eight-Stage Fluidized Beds", Intern. Chem. Eng. **17**, 254–259 (1977).

Schlingman, H., M.D. Wippern, H. Helmrich, and, K. Schugerl, Influence of Bed Structure and Tracer Sorption on the RTD in Fluidized Bed Reactors", in "Residence Time Distribution Theory in Chemical Engineering", A. Pethoe and R. D. Noble, Eds., Verlag Chemie GMbH, Weinheim (1982).

Schneider, P. and J.M. Smith, "Adsorption Rate Constant from Chromatograph", AIChE J. **13**, 886–895 (1968).

Sit, S.P. and J.R. Grace, "Effect of Bubble Interaction on Interphase Mass Transfer in Gas Fluidized Beds", Chem. Eng. Sci. **36**, 327–335 (1981).

Uysal, B.Z., I. Akşahin, and H. Yücel, "Sorption of $SO_2$ on Metal Oxides in a Fluidized Bed", Ind. Eng. Chem. Res. **27**, 434–439 (1988).

van Deemter, J.J. "Mixing and Contacting in Gas–Solid Fluidized Beds", Chem. Eng. Sci. **13**, 143–154 (1961).

van Der Laan, E.Th., "Notes on the Diffusion Type Model for the Longitudinal Mixing in Flow", Chem. Eng. Sci. **7**, 187–191 (1958).

van Swaaij, W.P.M., "Chemical Reactors", in "Fluidization", J.F. Davidson, R. Clift and D. Harrison, Eds., Academic Press, London, UK (1985).

Yoshida, K. and D. Kunii, "Stimulus and Response of Gas Concentration in Bubbling Fluidized Beds", Ind. Eng. Chem. Fundam. **1**, 11–16 (1968).

Zalewski, W.C. and D. Hanesian, "A Study of Dynamics of Gas Adsorption in Fixed and Fluidized Beds", AIChE. Symp. Ser. **69**, 58–67 (1973).



Manuscript received April 13, 2000; revised manuscript received October 24, 2000; accepted for publication November 1, 2000.